# Site-Selective Deposition and Micropatterning of $SrTiO_3$ Thin Film on Self-Assembled Monolayers by the Liquid Phase Deposition Method

Yanfeng Gao, Yoshitake Masuda, Tetsu Yonezawa, and Kunihito Koumoto*

*Department of Applied Chemistry, Graduate School of Engineering, Nagoya University, Nagoya 464-8603, Japan*

*Received May 13, 2002. Revised Manuscript Received September 4, 2002*

We have succeeded in site-selective deposition of $SrTiO_3$ (STO) thin films on patterned self-assembled monolayers (SAMs) by the liquid phase deposition (LPD) method. SAMs of heptadecafluoro-1,1,2,2,-tetrahydrodecyltrichlorosilanes [HFDTS, $CF_3(CF_2)_7(CH_2)_2SiCl_3$] were prepared on Si wafers and modified by UV irradiation through a photomask. This SAM template was composed of HFDTS surfaces ($Si-CF_3$) and silanol surfaces. The patterned SAM-covered substrate was then immersed into a $(NH_4)TiF_6/Sr(NO_3)/H_3BO_3$ aqueous solution at 50 °C to deposit a solid phase. $(NH_4)_2TiF_6$, which could form $[Ti(OH)_nF_{6-n}]^{2-}$ slowly in an aqueous solution, was selected as a source of $TiO_3^{2-}$. $H_3BO_3$ was a scavenger of fluorine and was used to control the reaction rate. The STO films were selectively deposited in the silanol regions. The as-deposited film was amorphous containing fluorine as a main impurity. With annealing at 500 °C for 2 h in air, the as-deposited film was crystallized into $SrTiO_3$ and the fluorine was eliminated. Film morphology was characterized by both SEM and AFM. Metal-oxide-semiconductor (MOS) devices were prepared by using an as-deposited film or a crystallized film as a gate oxide. The dielectric constant of $SrTiO_3$ thin films and the leakage current of the MOS device were evaluated. These results indicate that the $SrTiO_3$ film fabricated by a combination of the SAM technique with LPD method through a one-step process is promising for application to dielectric films.

## 1. Introduction

Perovskite-type materials of $ABO_3$, such as strontium titanate, barium titanate, and barium strontium titanate, are used in modern electronic devices. The $SrTiO_3$ (STO) thin film is a candidate dielectric material for capacitors in the next-generation dynamic random access memory (DRAM) with 1-Gbit density or higher, as well as in monolithic microwave integrated circuits (MMICs) because of its high dielectric constant (approximately 300).[1] It is also a candidate high-k dielectric to replace $SiO_2$ as a gate oxide film of MOSFETs.[2]

Several methods are used to prepare STO thin films, including RF magnetron sputtering,[3] metalorganic chemical vapor deposition (MOCVD),[4] molecular beam epitaxy (MBE),[5] pulsed laser deposition (PLD),[6] sol−gel,[7] and hydrothermal synthesis.[8] However, there are still processing issues to overcome before STO can be widely used in future electronic devices. Most vapor-deposition processing routes for film preparation can produce shaped material in a single step, but they require even higher energy than standard high-temperature processes.[9] Moreover, they cannot easily yield a thin film on a substrate with complex surface morphology or large surface area. The hydrothermal synthesis and sol−gel methods can produce thin films at low temperatures, but the former requires special equipment which is usually operated at high pressures, whereas the latter is a multistep process and many production parameters affect the quality of products. The challenge is to develop simple, energy-efficient, environment-friendly, and cost-effective processes for preparing STO thin films.

The liquid phase deposition (LPD) method is a low-cost, environment-friendly process for thin film preparation. LPD refers to the formation of oxide thin films from an aqueous solution of a metal−fluoro complex which is slowly hydrolyzed by adding water, boric acid ($H_3BO_3$), or aluminum metal.[10] The addition of water directly forces precipitation of the oxide, and boric acid or aluminum acts as a fluoride scavenger, destabilizing the fluoro complex and promoting precipitation of the oxide.

* Corresponding author. E-mail: g44233a@nucc.cc.nagoya-u.ac.jp. Tel: 81-52-789-3327. Fax: +81-52-789-3201.

(1) (a) Baba, S.; Numata, K.; Miyake, S. *Sci. Technol. Adv. Mater.* **2001**, *1*, 211. (b) Kunihisa, T.; Yamamoto, S.; Nishijima, M.; Yokohama, T.; Nishituji, M.; Nishii, K.; Ishikawa, O. *IEICE Trans. Electron.* **1999**, E82-C, 1921.

(2) Wilk, G. D.; Wallace, R. M.; Anthony, J. M. *J. Appl. Phys.* **2001**, *89*, 5243.

(3) Song, M. H.; Lee, Y. H.; Hahn, T. S.; Oh, M. H.; Yoon, K. H. *J. Appl. Phys.* **1996**, *79*, 3744.

(4) Hahn, Y. B.; Kim, D. O. *J. Vac. Sci. Technol.* **1999**, *A17*, 1982.

(5) Tsurumi, T.; Suzuki, T.; Yamaze, M.; Daimon, M. *Jpn. J. Appl. Phys.* **1994**, *33*, 5192.

(6) Tachiki, M.; Noda, M.; Yamada, K.; Kobayashi, T. *J. Appl. Phys.* **1998**, *83*, 5351.

(7) Klee, M.; Mackens, U. *Microelectron. Eng.* **1995**, *29*, 185.

(8) Yoshimura, M.; Suchanek, W. L.; Watanabe, T.; Sakurai, B. *J. Euro. Ceram. Soc.* **1999**, *19*, 1353.

(9) Yoshimura, M.; Suchanek, W. L.; Byrappa, K. *Mater. Res. Bull.* **2000**, *25*, 17.

(10) Deki, S.; Aoi, Y.; Asaoka, Y.; Kajinami, A.; Mizuhata, M. *J. Mater. Chem.* **1996**, *7*, 733.

10.1021/cm020358p CCC: $22.00 
Published on Web 11/12/2002

The LPD method was first developed for depositing $SiO_2$ thin films, and was later used to prepare simple oxides, such as $TiO_2$,[10] $V_2O_5$, $VO_2$, FeOOH ($Fe_2O_3$),[11] and multicomponent metal oxide films.[12] However, no LPD deposition of STO has been reported. The key technique in LPD is to prepare films by means of the ligand-exchange (hydrolysis) equilibrium reaction of metal−fluoro complex species. The addition of boric acid or aluminum serves merely to control the reaction rate. The LPD method may enable individual components to be mixed on a molecular level and offers strict control over stoichiometry.

Adapting some of the key features of the biomineralization process, self-assembled monolayers (SAMs) have been used to tailor the chemical characteristics of substrate surfaces by producing highly specific interfaces spread over relatively large areas, which also can be modified chemically or physically to generate surfaces having different reactivity and properties. A commonly used method is UV-irradiation through a photomask. The modified SAMs can then be employed as templates to fabricate micropatterns of functional materials and small devices of the required size and shape with outstanding precision through a one-step process at room temperature.

Direct deposition and micropatterning of functional ceramic thin films has been achieved for anatase $TiO_2$ thin films using the LPD method and employing a patterned phenyltrichlorosilane SAM.[13] Selective deposition of amorphous $TiO_2$ thin films with high resolution has been further demonstrated by means of the nonaqueous solution method[14] or through gas-phase reactions.[15] This novel method has enabled the preparation of micropatterns, manipulation of material surfaces, and creation of materials in the form of a film through a one-step process at ambient temperature.

The purpose of this study is to selectively deposit STO thin films by combining the LPD method with the SAM patterning technique. In an LPD process, any compound that can react with $F^-$ or any form of hydrolysis product of $[TiF_6]^{2-}$, can shift the reaction equilibrium toward the oxide deposition. If an $Sr^{2+}$ source is added into the aqueous solution of $(NH_4)TiF_6$ and Sr−O−Ti bonds that are more stable than Ti−O−Ti can be formed, the oxide deposition reaction can proceed and produce strontium titanate (STO). To directly deposit a high-quality STO thin film by means of LPD, $(NH_4)_2TiF_6$ which can generate $[Ti(OH)_nF_{6-n}]^{2-}$ slowly in the aqueous solution was selected as a source of $TiO_3^{2-}$, and $H_3BO_3$ was used to control the reaction rate.

The dielectric properties of the STO film were evaluated by measuring the capacitance−voltage (C−V) and current−voltage characteristics (I−V) of the MOS device. The dielectric constants of the as-deposited film and the crystallized one were obtained. The insulating properties and leakage current of the MOS device were also evaluated.

(11) Deki, S.; Aoi, Y. *J. Mater. Res.* **1998**, *13*, 883, and references therein.
(12) Yao, T.; Uchimoto, Y.; Sugiyama, T.; Nagai, Y. *Solid State Ionics* **2000**, *135*, 359.
(13) Koumoto, K.; Seo, S.; Sugiyama, T.; Seo, W. S.; Dressick, W. J. *Chem. Mater.* **1999**, *11*, 2305.
(14) Masuda, Y.; Sugiyama, T.; Lin, H.; Seo, W. S.; Koumoto, K. *Thin Solid Films* **2001**, *382*, 153.
(15) Masuda, Y.; Seo, W. S.; Koumoto, K. *Langmuir* **2001**, *17*, 4876.

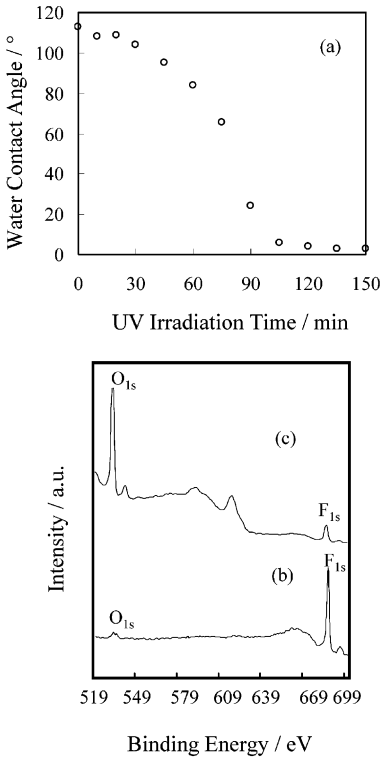


**Figure 1.** Water drop contact angle of HFDTS-SAMs as a function of UV-irradiation time (a), and XPS spectra of HFDTS-SAMs before UV-irradiation (b), along with that of HFDTS-SAMs UV-irradiated for 3 h (c).

## 2. Experimental Section

**SAM Preparation and Modification.** P-type Si (100) wafers (Shinetsu; resistivity 5−10 Ωcm) employed for the substrates were cleaned ultrasonically in acetone, ethanol, and deionized water (>17.6 MΩcm), followed by immersion in boiling water for 5 min. Heptadecafluoro-1,1,2,2,-tetrahydrodecyltrichlorosilane (HFDTS)-SAM was prepared by immersing the cleaned and dried substrate into an anhydrous toluene (99.8%, water < 0.002%, Aldrich) solution containing 1 vol % HFDTS (Aldrich) for 5 min under an $N_2$ atmosphere. After being dried under the $N_2$ atmosphere, the substrate with SAM was then baked at 120 °C for 5 min to remove residual solvent and to promote chemisorption of the SAM.

SAMs were exposed for 3 h to UV light (184.9 nm) from a low-pressure Hg lamp (5 W × 4 Hg lamps, NL-UV253, Nippon Laser & Electronics Lab) through a photomask, which selectively modified the functional groups of the exposed areas while leaving the rest unchanged. The UV-irradiation process resulted in the formation of a patterned SAM with hydrophilic silanol (Si−OH) regions in the exposed area and hydrophobic heptadecafluoro regions in the nonirradiated areas. Water drop contact-angle measurement (CA-D, Kyowa Interface Science) and XPS analysis (ESCA-3200, Shimadzu; pass energy: 75 eV) were conducted to check the successful formation of HFDTS-SAM and the cleavage of functional groups by UV-irradiation. HFDTS-SAM without UV-irradiation showed a water-contact angle of 115°, but after UV-irradiation the angle changed to less than 5° (Figure 1a). Accompanied by dramatic weakening of $F_{1s}$ intensity compared to that for the as-prepared HFDTS-SAMs (Figure 1b), an $O_{1s}$ peak with increasing intensity in the XPS spectrum after UV-irradiation for 3 h confirmed the formation of silanol groups by UV-irradiation (Figure 1c).

**Deposition of STO Films.** The starting materials employed were ammonium hexafluorotitanate [$(NH_4)_2TiF_6$ (AHFT), 98.5%, Mitsuwa Chemical Co., Japan], boric acid (BA) and strontium nitrate (SN) (purity 98%, Kishida Chemical Co., Japan). All reagents were used in the as-received form without further purification. They were separately dissolved in deion-

ized water and then mixed to form a homogeneous solution containing 15−25 mM AHFT, 15−25 mM SN, and 45−75 mM BA. The typical molar ratio was AHFT/SN/BA = 1−1.3:1−1.3:3. The deposition of a solid phase was conducted by immersing the patterned SAM-covered substrate into the solution at 50 °C for 30 min − 7 h. The substrate was placed at the bottom of the solution or floated on the surface of solutions with the SAM upside down to prevent particles formed in the solution from accumulating on the substrate surface. The substrate with a deposit was rinsed carefully in distilled water before air-drying.

**Characterization Techniques.** A scanning electron microscope (SEM; model S-3000N, Hitachi) was used to observe the deposits and precipitates on the substrate. A scanning probe microscope (SPI3800N, Seiko Instruments Inc.) was operated in AFM mode to observe the topography of the films; scans were taken at room temperature under ambient air with a frequency of 1 kHz. The chemical composition of the deposited film was analyzed by X-ray photoelectron spectroscopy (XPS; Escalab210, VG Scientific Ltd.) with Mg Kα as the X-ray source operated at constant pass energy of 20 eV. All spectra were referenced to the $C_{1s}$ signal at 284.6 eV. The structure and phase composition were characterized by X-ray diffraction (XRD; model RAD-1C, Rigaku) with Cu Kα radiation ($\lambda$ = 0.15418 nm) at a scanning speed of 1°/min. Fourier transform infrared (FT-IR) measurement, by a Jasco FT/IR-610 equipped with a TGS detector, was conducted to further characterize the collected precipitate after depositing STO precursor solid thin films. Spectra were taken at a resolution of 4 $cm^{-1}$ by using KBr as reference. The thickness of films was measured by a laser ellipsometer (PZ2000, Philips) with an incidence angle of 70° and wavelength of 632.8 nm. Gold was evaporated onto both the as-deposited film ($0.785 \times 10^{-6}$ $m^2$) and the rear side of a Si wafer (approximately $1.225 \times 10^{-5}$ $m^2$) to form electrodes for a MOS device. A source measurement unit (KEITHLEY236) and an impedance analyzer (HP4192A) were employed to measure the dielectric properties of the MOS device.

## 3. Results and Discussion

**Film Growth Conditions.** Hereafter AHFT, SN, and BA refer to ammonium hexafluorotitanate, strontium nitrate, and boric acid, respectively. A suitable supersaturated solution is needed for the deposition of high-quality thin films. When the molar ratio of AHFT/SN/BA was 1:1:0 or 1:1:1, the solution was so stable that a long soaking time was needed to deposit films. A typical film deposited in 25 mM AHFT−SN aqueous solution without BA after soaking for 32 h showed that the deposit was an unidentified crystalline solid and transformed to STO after annealing at 600 °C for 2 h in air. However, a solution of AHFT/SN/BA = 1:1:5 was unstable, so precipitation occurred immediately after they were mixed. The molar ratio of AHFT/SN/BA was then defined as 1:1:3 (pH approximately 3.40). The deposition solution consisted of 0.025 M AHFT, 0.025 M SN, and 0.075 M BA, unless otherwise noted. The deposition temperature was kept constant at 50 °C. In this solution, obvious homogeneous precipitation occurred after soaking for 30 min. The pH of the solution changed slightly (i.e., from 3.40 to 3.35), which was attributed to the weak acidity of $HBF_4$ generated by AHFT hydrolysis in the presence of boric acid.

The color of the silanol surface with deposits, which was golden yellow after 2 h of soaking by placing the substrate at the bottom of the solution and blue for the species obtained by floating substrates over the solution, suggested that the material was deposited on the silanol regions. XRD measurement in Figure 2 confirmed that

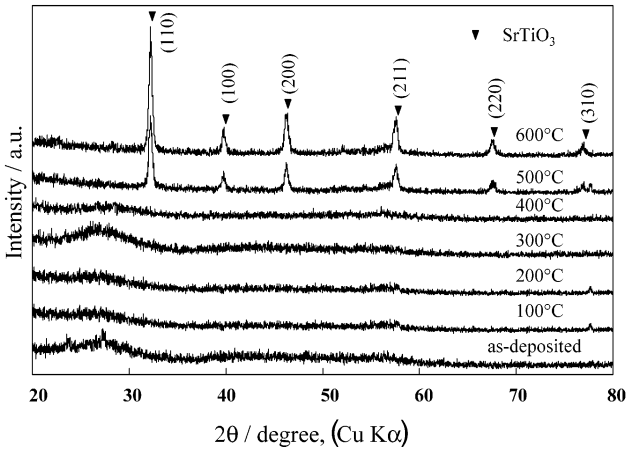


**Figure 2.** XRD profiles of the $SrTiO_3$ thin film deposited on the silanol surfaces for 2 h in 0.025 M $(NH_4)_2TiF_6$/0.025 M $Sr(NO_3)_2$/0.075 M $H_3BO_3$ aqueous solution at 50 °C, and those after annealing at different temperatures for 2 h in air (JCPDS Card: 350734).

the as-deposited films were amorphous and remained in the amorphous state up to 400 °C, which is rather different from anatase deposited without $Sr(NO_3)_2$.[13] For deposition of $TiO_2$ on the SAM surface through the LPD method, we obtained crystallized anatase $TiO_2$ thin films,[13] but we could get only an amorphous STO precursor solid under the present conditions. Crystallization of the as-deposited STO precursor solid into STO was detected after annealing at 500 °C for 2 h in air. The STO exhibited good crystallinity after annealing at 600 °C. The crystallite size was calculated by Scherer's equation ($S = K\lambda/(\beta\cos\theta)$), where $K$, $\lambda$, $\beta$, and $\theta$ denote the Scherrer constant (= 0.89), wavelength (0.15405 nm) of Cu Kα radiation, integrated width (0.09412 rad) of the peak profile, and Bragg angle of diffraction peak ($2\theta$ = 32.2°), respectively. The mean crystallite size after annealing at 600 °C for 2 h (Figure 2) is not larger than 2 nm. Figure 2 also shows only diffraction peaks from STO. The diffraction peaks of STO after annealing became strong, and the full-width at half-maximum became small, suggesting that better crystallinity was obtained at 600 °C. Even if the molar ratio of AHFT/SN/BA was changed from 1:1:3 to 1.3:1:3 or 1:1.3:3, the XRD pattern for the samples annealed at 600 °C for 2 h in air showed only STO diffraction peaks. No peaks corresponding to $TiO_2$ were observed. Further changing the molar ratio of AHFT/SN/BA to 1:2:3 or 2:1:3, prolonging the soaking time to 12 h, and heating the samples at 800 °C for 1 h, no peaks except those of STO appeared. The samples were then subjected to XPS for quantitative analysis. For such measurement, the samples were $Ar^+$-bombarded for 30 min to remove the contamination of the surface. Thus, the result of XPS could represent the composition in the film, not in the surface of the film. The atomic ratio of Sr/Ti = 1.0:1.04 (by XPS analysis) for a specimen derived from a starting ratio of SN/AHFT = 1:1.3 further confirmed that films with nearly stoichiometric composition tend to deposit. No $Si_{2p}$ signals for both the samples soaked for 1 and 2 h were detected by XPS, suggesting that the film completely covered the substrate. For the film obtained by placing the substrate horizontally at the bottom of a solution, $Si_{2p}$ signals were shielded even after 30 min of deposition. Film deposited

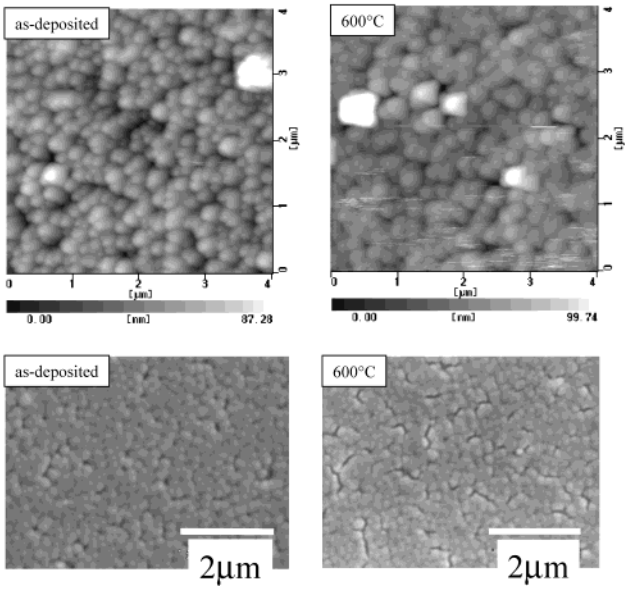


**Figure 3.** AFM images and SEM photographs of the as-deposited STO film on the silanol surfaces and that after annealing at 600 °C for 2 h in air. (Deposition conditions same as in Figure 2, substrates were floated.)

on the immersed substrate was notably thicker than that deposited on the floating substrate: i.e., after soaking for 2 h, 192.3 nm thick for the film deposited by floating the substrate and 248.6 nm thick for that obtained by immersing the substrate.

The surface morphology and topography of films formed in the silanol regions were analyzed by SEM and AFM, respectively. Figure 3 shows the AFM images and SEM photographs of the as-deposited film (50 °C, 2 h) on the floated silanol surface of modified HFDTS-SAMs and that after heating at 600 °C for 2 h in air. The AFM image reveals the formation of a uniform film of densely packed particles. The particle size is about 200 nm. The roughness of RMS for the whole measured area (about $4 \times 4$ $\mu$m) is 10.6−12.9 nm depending on the investigated area. Such topography and roughness are typical for the whole specimen and were easily reproduced. Moreover, after soaking for 1 h or longer, no significant difference in topography was observed. It seems that Ostwald ripening growth in the very initial stage of deposition might have affected the topography of the final film. This observation also suggested that films formed primarily via the deposition of particles originally formed in the solution, which was consistent with the XRD result that the film was composed of randomly oriented particles. The topography of films after annealing at 300 °C for 2 h in air (images not shown) did not exhibit an obvious difference compared to that of the as-deposited films observed by AFM, whereas annealing at 600 °C resulted in not only crystallization (Figure 2) but also grain growth and densification (Figure 3). Conversely, the difference in grain morphology and size for the as-deposited film and a corresponding one annealed at 600 °C was reflected in the dielectric properties of the film, which will be discussed further in a later section. After annealing at 600 °C for 2 h in air, cracks could be observed in an SEM photograph of Figure 3, but the rather low leakage current for the same film (see the dielectric properties section) suggested that the cracks were superficial and did not extend throughout the film; although direct observation of a cross section was not successful. Note that no efforts were made to optimize the annealing process.

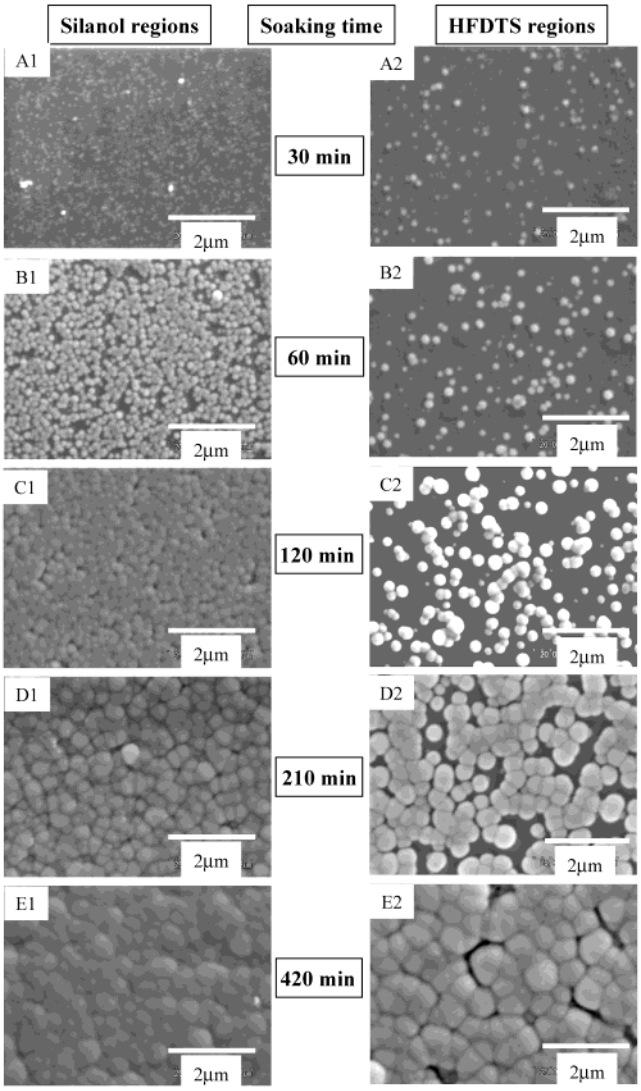


**Figure 4.** SEM photographs of deposition with soaking time in the HFDTS regions and silanol regions. (Deposition conditions same as in Figure 2, substrates were floated.)

**Site-Selective Deposition and Micropatterning.** When UV-modified HFDTS-SAMs (silanol surfaces) along with nonirradiated ones (HFDTS surfaces) were immersed into the SN-AHFT-BA solution, site-selective deposition of STO films occurred. The SEM photographs of Figure 4 show the variation of deposition rate on the silanol and HFDTS surfaces with soaking time. The substrates were floated over the surface of the solution with the SAM surface upside down. The induction period of silanol surface was much shorter than that on the hydrophobic HFDTS surface. Small or large dot-like deposits could be clearly observed on the silanol surface after deposition for as short as 30 min (Figure 4A1) and an increase in its number could be observed by prolonging the soaking time to 60 min (Figure 4B1). Particles were further coalesced to form a thin film (Figure 4C1−E1) as the deposition proceeded. The thickness for a typical dense film on the silanol surface after soaking for 2 h was about 200 nm, which was confirmed by both SEM and ellipsometry.

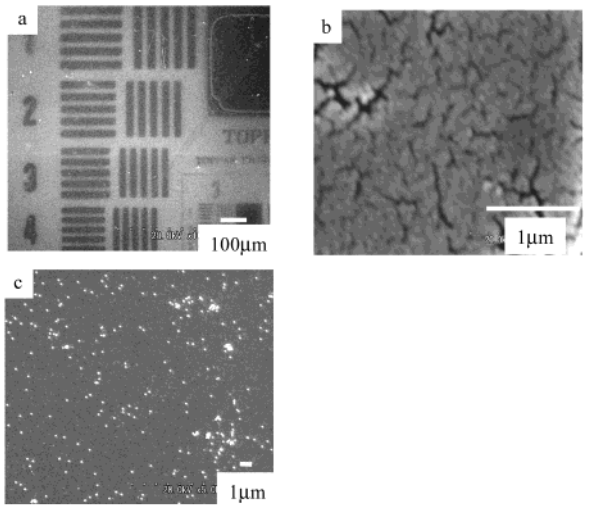


**Figure 5.** SEM photographs of the STO thin film deposited on a micropatterned HFDTS-SAM in 0.015 M $(NH_4)_2TiF_6$/0.015 M $Sr(NO_3)_2$/0.045 M $H_3BO_3$ solution at 50 °C for 2.5 h (a), and enlarged photographs of film on the silanol region (b) and on the HFDTS region (c).

In contrast, on the HFDTS surface, film formation was postponed (Figure 4A2−E2). Obvious white dot-like particles were observed after soaking for 30 min (Figure 4A2) but much less in number than that in the silanol surface. After soaking for 3.5 h, a film with large cavities could be observed (Figure 4D2). After soaking for 7 h, no obvious difference could be observed for the film on the silanol surface and HFDTS surface by SEM and the regions became almost indistinguishable. But in the 50 °C air-dried film on the HFDTS surface, obvious cracks or partial peeling off of the film from the substrate were observed (Figure 4E2), while a crack-free film was obtained on the silanol surface. This result also shows that the selectivity under these conditions is not sufficient to prepare a high-resolution micropattern with 100% coverage difference.

We can infer that the film formation mechanism in this case is three-demensional or Ostwald ripening growth mode and not layer-by-layer mode, that is, particulates growing with consummation of smaller ones, which does not imply a surface-promoted heterogeneous mechanism of nucleation but rather nucleation in the solution followed by particle adsorption to the SAM surface. This also implies that the thickness of the film mainly depends on the particle size. Small particle size will result in not only a thinner film but also an increase in film density, which may be reflected in improved dielectric properties, such as high capacitance and low leakage current.

As Figure 4 shows, processing conditions such as pH value, concentration, and deposition temperature should be controlled to achieve a high-resolution pattern. Figure 5 shows SEM photographs of the micropatterns obtained by depositing for 2.5 h in a 15 mM AHFT, 15 mM SN, and 45 mM BA solution at pH of approximately 3.4 controlled by the addition of an appropriate amount of $HNO_3$. The solution was transparent during deposition. After deposition, the film was rinsed by supersonic cleaning for 1 min to peel off loose particles, especially those deposited on the HFDTS regions. As shown in Figure 5, STO precursor solid films were selectively deposited on the silanol regions (dark areas) in contrast

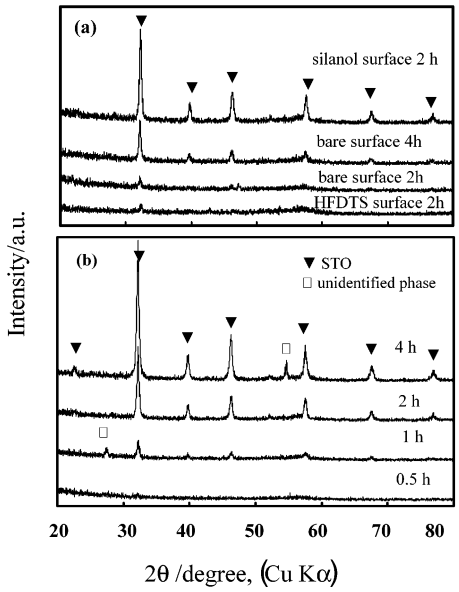


**Figure 6.** XRD profiles of (a) the STO thin film deposited on the various surfaces for different soaking times, and (b) STO film deposited on the silanol surfaces with various soaking times; all samples were deposited at 50 °C in the same solution as in Figure 2 and annealed at 600 °C for 2 h in air.

to hydrophobic HFDTS regions (gray-white areas). However, the resolution for the current micropatterns is much lower compared to that for the amorphous micropatterns of $TiO_2$[14,15] and $ZrO_2$[16] that we produced by an organic solution method. Further efforts should be made to improve the resolution, and investigations are now underway.

The XRD measurements in Figure 6 show that the selectivity of deposition varies with different surfaces (Figure 6a), and that the growth rate of films in the silanol surfaces varies with soaking time (Figure 6b). All the samples were annealed at 600 °C for 2 h in air. For the bare p−Si substrate (without SAMs), small peaks for STO can be observed after deposition for 2 h, followed by obvious diffraction peaks after deposition for 4 h. In the hydrophobic HFDTS surface, after deposition for 2 h, the diffraction peak ($2\theta = 32.2°$) was smaller than that observed on the bare substrate. In contrast, on the hydrophilic silanol surface, stronger diffraction peaks after deposition for 2 h suggest a thicker film than the bare surface. Lengthening the soaking time, as shown in Figure 6b, resulted in stronger relative intensity of the diffraction peaks, suggesting that the thickness of the film increased. In fact, thicknesses of the films deposited on silanol surfaces for 1, 2, 3, and 4 h were measured by ellipsometry to be 101.3 nm, 165.5, 205.4, and 230.0 nm, respectively. However, on the HFDTS surface, film with 100% coverage did not form after soaking for 2 h (Figure 4C2). A typical thickness for 4 h soaking was 125.6 nm. These results indicate that growth of the film was significantly promoted on the silanol surface.

**Chemical Composition and Reaction Mechanism.** The chemical composition of the as-deposited film was further characterized by XPS and FT-IR. XPS (Figure 7) measurement for a film deposited on a silanol

(16) Gao, Y.; Masuda, Y.; Yonezawa, T.; Koumoto, K. *J. Ceram. Soc. Jpn.* **2002**, *110*, 379.

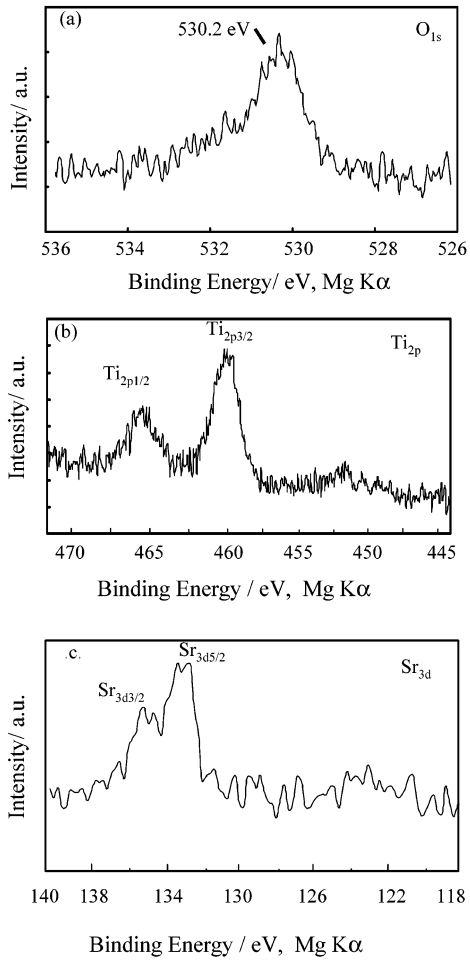


**Figure 7.** XPS spectra of $O_{1s}$ (a), $Ti_{2p}$ (b), and $Sr_{3d}$ (c) for the as-deposited STO thin films on the silanol surfaces of UV-modified HFDTS-SAM. (Deposition conditions same as in Figure 2.)

surface shows that the binding energies for $Sr_{3d5/2}$, $Ti_{2p1/2}$, $Ti_{2p3/2}$, and $O_{1s}$ were 133.5 eV, 465.5, 459.0, and 530.2 eV, corresponding to $Sr^{2+}$, $Ti^{4+}$, and $O^{2-}$, respectively.[17] Those peaks remained almost without shift during annealing at 100 to 600 °C for 2 h in air (spectra not shown) compared to those of the as-deposited film. The binding energies for $O_{1s}$ after STO crystallized were higher than that of 529.0 eV for a single crystal,[17a] probably suggesting a difference between the structures of thin films and single crystal. No $N_{1s}$, $Si_{2p}$, or $B_{1s}$ peak was detected. We can infer that $Sr^{2+}$ ions in the as-deposited film are not present as Sr species containing nitrogen such as $Sr(NO_3)_2$, which has been proposed for potentiostatic electrochemical deposition of $BaTiO_3$ film.[18] However, an obvious peak (Figure 8) located at about 684.7 eV (corresponding to $F_{1s}$) suggested that the as-deposited film contained a certain quantity of fluorine. The heating process resulted in complete elimination of fluorine after annealing at 500 °C (Figure 8) and decomposition of the as-deposited STO precursor solid into crystallized $SrTiO_3$, certified by the result of XRD.

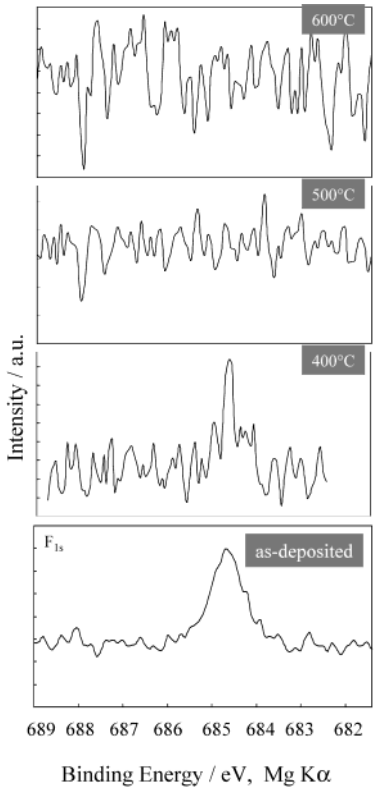


**Figure 8.** XPS spectra of $F_{1s}$ for the as-deposited STO thin film and those after annealing at different temperatures.

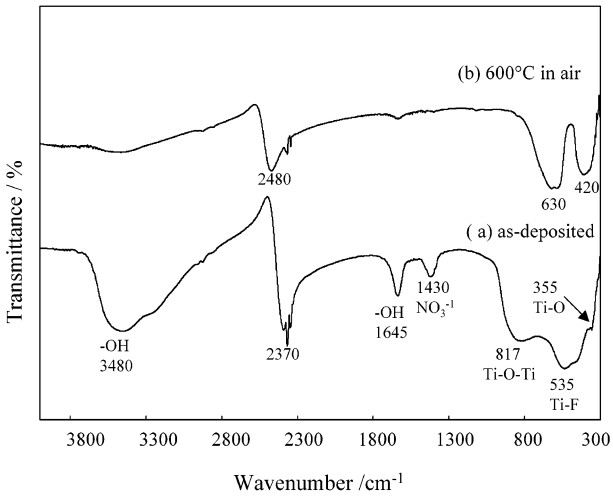


**Figure 9.** FT-IR spectra of (a) amorphous precipitate collected after depositing thin films and (b) that after annealing at 600 °C for 2 h in air.

FT-IR measurement for the as-deposited amorphous powder is shown in Figure 9. A band at around 355 $cm^{-1}$ is attributed to Ti−O stretching in titanates.[19] For the as-obtained precipitate (Figure 9a), a clear band at around 535 $cm^{-1}$ is characteristic of the Ti−F stretching mode.[20] A broad band at about 817 $cm^{-1}$ suggests the presence of −Ti−O−Ti−O chains.[19b] Bands at 1645 $cm^{-1}$ and 1430 $cm^{-1}$ are due to adsorbed water and residual $NO_3^-$, respectively.[21] A band at around 3480

(17) (a) Shibagaki, S.; Fukushima, K. *J. Euro. Ceram. Soc.* **1999**, *19*, 1423. (b) Adachi, Y.; Kohiki, S.; Wagatsuma, K.; Oku, M. *Appl. Surf. Sci.* **1999**, *143*, 272.

(18) Nomura, K.; Shibata, N.; Maeda, M. *J. Ceram. Soc. Jpn.* **2001**, *109*, 915.

(19) Leite, E. R.; Sousa, C. M. G.; Longo, E.; Varela, J. A. *Ceram. Inter.* **1995**, *21*, 143.

(20) (a) Laptash, N. K.; Maslennikova, I. G.; Kaidalova, T. A. *J. Fluorine Chem.* **1999**, *99*, 133. (b) Sengupta, A. K.; Adhikari, S. K.; Dasgupta, H. S. *J. Inorg. Nucl. Chem.* **1979**, *41*, 161.

(21) Klingenberg, B.; Vannice, M. A. *Chem. Mater.* **1996**, *8*, 2755.

$cm^{-1}$ is attributed to hydroxyl group stretching.[21] A band located at 2370 $cm^{-1}$ cannot be assigned to stretching of nitrate, borate, fluorine, or carbonate, but is still unidentified. After annealing at 600 °C (Figure 9b), 420 and 640 $cm^{-1}$ are characteristic of the Ti−O stretching mode in STO.[19] The peaks at 3480 and 535 $cm^{-1}$ disappeared, consistent with the decomposition of hydroxide group and fluorine species. On the basis of the XPS and FT-IR results, it is clear that fluorine existed in the structure of the as-deposited film, most probably in the form of $Sr[TiF_{6-n}(OH)_n]$. Our as-deposited STO films were amorphous as discussed before and contained significantly larger amounts of fluorine than the anatase film.[22] The deposition rate of STO was found to be higher than that of anatase. These findings reveal that the hydrolysis reaction of AHFT in deposition of STO did not proceed as smoothly as in the deposition of anatase, probably because Sr species reacted with some intermediate hydrolyzed species. Preferential hydrolysis of AHFT before it is mixed with $Sr(NO_3)_2$ might minimize the residual fluorine, and so our low-temperature deposition method may be a more environment-friendly process for industrial applications.

The sequence of reactions for the formation of STO films is expected to be as follows.

1. Hydrolysis of dissociated AHFT salt

$$TiF_6^{2-} + n\ H_2O \leftrightarrow [TiF_{6-n}(OH)_n]^{2-} + n\ HF \quad (1)$$

$$[TiF_{6-n}(OH)_n]^{2-} \xrightarrow{OH^{-1}} [TiF_{5-n}(OH)_{n+1}]^{2-} + F^- \xrightarrow{(5-n)\ OH^{-1}} [Ti(OH)_6]^{2-} + 5\ F^- \quad (2)$$

and promotion of hydrolysis by BA:

$$H_3BO_3 + 4\ HF \leftrightarrow BF_4^- + H_3O^+ + 2\ H_2O \quad (3)$$

2. Formation of STO precursor solid

$$Sr^{2+} + [TiF_{6-n}(OH)_n]^{2-} \rightarrow Sr[TiF_{6-n}(OH)_n], \quad (4)$$

$$\text{or } Sr^{2+} + [TiF_{6-n}(OH)_n]^{2-} \rightarrow Sr[TiF_{6-n}O_{m/2}(OH)_{n-m}] + m/2\ H_2O \quad (5)$$

3. Decomposition of STO precursor solid into STO by annealing at > 500 °C

$$Sr[TiF_{6-n}(OH)_n] \rightarrow SrTiO_3 + (n-3)\ H_2O + (6-n)\ HF \quad (6)$$

The $TiF_6^{2-}$ ion is stable in water,[23] but still hydrolysis reaction occurs. For $TiF_6^{2-}$ to hydrolyze in water, an acid solution is required, because the formation of a hydrogen bond to fluorine weakens the Ti−F bond.[23b] At pH 3.4, as shown in eq 1, hydrolysis of the $TiF_6^{2-}$ takes place by a ligand-exchange equilibrium reaction.[10,23] The value of $n$ is small and the degree of hydrolysis ($\eta$) decreases by increasing the concentration of $TiF_6^{2-}$; typically for a 0.02 M $TiF_6^{2-}$ aqueous solution (pH = 3.42), $\eta$ is only 0.06.[10,23] By adding $H_3BO_3$ as $F^-$ scavenger, the eq 1 is accelerated and the equilibrium shifts to the right-hand side because of the $F^-$ consumption reaction. $H_3BO_3$ readily reacts with $F^-$ by formation of stable cations including $HBF_4$.[24] Reactions occur stepwise and one of these steps as shown in eq 3 is slow.[10,24] It is obvious that hydrolysis of AHFT, especially formation of $HBF_4$, is the rate-limiting reaction to generate species of $[TiF_{6-n}(OH)_n]^{2-}$. The pH of the solution after soaking for 2 h in our experiment slightly decreased from 3.40 to 3.35 due to the formation of $HBF_3(OH)$ and $HBF_4$, both of which demonstrate the weak acidity.[23]

Stoichiometry of STO precursor solid films, even at different molar ratios of starting materials, firmly suggests that the as-deposited STO precursor solid should be a compound with Sr−O−Ti bonds, rather than a coprecipitated mixture of Sr species and Ti species. Possible deposition mechanism of such STO precursor solid was represented as eqs (4) and (5). The as-deposited STO precursor solid was then decomposed into STO by annealing as shown in eq 6.

To understand the adhesion mechanism of particles to the SAM surface, the Scotch-tape adhesion peel test was carried out. No difference was observed in the optical micrograph of films on the silanol surface before and after the Scotch-tape adhesion peel test, which showed that the deposit could not be peeled off. The film on the silanol regions could not be completely torn off by ultrasonic cleaning (150 W) for 10 min, which suggested strong adhesion of the STO film by strong chemical bonds formed between STO and silanol regions. Particles originally formed in the solution may site-selectively react with −OH terminated silanol groups by the formation of strong chemical bonds. However, the nonreactive hydrocarbon chains make it impossible to create chemical bonds in the HFDTS regions. It is, therefore, considered that the different interfacial interactions between the substrate and the deposited particles may be attributed to the various adhesion strengths. The ultrasonic cleaning should have eliminated loose deposits in the hydrophobic regions, thus improving the resolution of micropatterns.

**Partial Charge Model and Complexation of Ti(IV).** The partial charge model, based on Sanderson's principle of electronegativity equalization in a compound, is a simple qualitative model for understanding the behavior of an element during hydrolysis, condensation, and complexation. Condensation of cations in the solution can occur only when the hydroxo ligand in the coordination sphere of the cation is present.[25] Two main mechanisms as schematically shown below are involved in the condensation of cations: olation reaction and oxolation reaction taking place by formation of hydroxo bridges (ol bridges) and oxo bridges, respectively.

$$\text{olation: } M{-}OH + {-}M - OH_2 \rightarrow M{-}OH{-}M{-} + H_2O$$

$$\text{oxolation: } M{-}OH + HO - M \rightarrow M{-}O{-}M + H_2O$$

(22) Kishimoto, H.; Takahama, K.; Hashimoto, N.; Aoi, Y.; Deki, S. *J. Mater. Chem.* **1998**, *8*, 2019.

(23) (a) Schmitt, R. H.; Grove, E. L.; Brown, R. D. *J. Am. Chem. Soc.* **1960**, *82*, 5292. (b) Buslaev, Y. A.; Dyer, D. S.; Ragsdale, R. O. *Inorg. Chem.* **1967**, *6*, 2208.

(24) (a) Mesmer, R. E.; Palen, K. M.; Bases, C. F., Jr. *Inorg. Chem.* **1973**, *12*, 89. (b) Wamser, C. A. *J. Am. Chem. Soc.* **1951**, *73*, 49. (c) Wamser C. A. *J. Am. Chem. Soc.* **1948**, *70*, 1209.

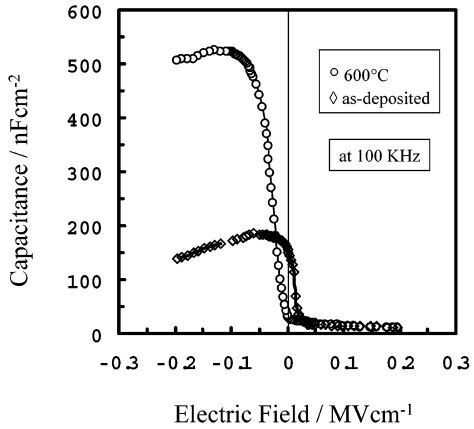


**Figure 10.** High-frequency (100 kHz) C−V characteristics of the MOS device with the crystallized STO film (annealing at 600 °C for 2 h in air) and the as-deposited precursor solid STO thin film as gate films.

Condensation through the mechanism of either olation or oxolation depends on the electronegativity of the element involved.[25] Briefly, four critical values, $\chi_{B,z}$, $\chi_{Ol}$, $\chi_{PA}$, and $\chi_A$, separate the charge−electronegativity diagram into five domains (*B*, *z*, Ol, PA, and *A*, which mean base, formal charge, olation, polyacid, and acid, respectively). When $\chi^*_M$ (the electronegativity of hydrolyzed cation) > $\chi_A$ or $\chi^*_M < \chi_{B,z}$, condensation in the solution cannot occur and the element will exist as a monomeric cation or anion. $\chi_{B,z} < \chi^*_M < \chi_{Ol,z}$ limits a domain where cations may condense through olation only and forms stable hydroxides (e.g., Al, Zn). If $\chi_{Ol,z} < \chi^*_M < \chi_{PA,z}$, condensation may occur through both olation and oxolation and lead to oxyhydroxides [Fe(III)] or to oxides [Ti(IV)] depending upon the relative rate of olation and oxolation. Elements for which $\chi_{PA,z} < \chi^*_M < \chi_{A,z}$ will condense through oxolation, leading to polyacid formation.

Niesen et al.[26] applied the partial charge model to measure electronegativity−pH diagrams of complexants of titanium species by chlorine and fluorine for the deposition of $TiO_2$ thin film. Their results show that stable fluorine complexes of titanium (IV) could be formed under acid conditions. In our reaction system, following $F^-$ release, a series of hydrolysis species formed. Let us consider a species of $[TiF_2(OH)_4]^{2-}$ as an example. According to the electronegativity analysis, $\chi$(HF) for HF species, $\chi(F_2^{2-})$ for the species $F_2^{2-}$, $\chi(D)$ for average electronegativity of the entity $[Ti(OH)_4]^0$, and $\chi(H)$ for the average electronegativity of $[Ti(OH)_6]^{2-}$, are 2.934, 1.346, 2.501, and 2.23, respectively. It is obvious that $\chi(F_2^{2-}) < \chi(D)$ and $\chi$(HF) > $\chi(H)$, which suggests the complex ions of $[Ti(OH)_4F_2(H_2O)_2]^{2-}$ are stable in our solution system.

**Dielectric Characteristics of STO Films.** Figure 10 shows high-frequency (at 100 kHz) C−V characteristics taken over the range of +4 V to −4 V for a crystallized film obtained by annealing at 600 °C for 2 h in air and that for an as-deposited film. The C−V characteristics were generated by sweeping the MOS capacitor from the inversion to accumulation state. The accumulation region of the C−V curve is observed when negative voltages are applied to the gate. The negative polarity causes majority carriers (holes) to be attracted toward the gate and accumulate at the substrate−oxide interface. As the gate voltage moves toward a positive value, holes are repelled from the substrate−oxide interface and a carrier-depleted area forms beneath the oxide, creating an insulator because of the absence of free-moving charges. In the inversion region, the positive gate voltage both generates electron−hole pairs and attracts the minority carriers (electrons), which accumulate at the substrate−oxide interface to form an inversion layer. The corresponding depletion region reaches the maximum depth, and the slope of the C−V curve becomes almost flat at 100 kHz. The maximum constant capacitance of 4.2 nF for the crystallized film was obtained when the MOS device of Au/STO/$SiO_2$/p-Si/ was in the ON-state. The dielectric constant ($k_{STO}$) of 179 was determined using the following relationship

$$k_{STO} = d_{STO}/(k_0 S/C - d_{SiO2}/k_{SiO2})$$

where *C* is the maximum capacitance at negative bias voltage (4.2 nF), $d_{STO}$ (= 203.2 nm, by ellipsometry) and $d_{SiO2}$ (= 2 nm) are the thicknesses of STO and $SiO_2$ layer, respectively; *S* is the area of the Au electrode ($0.785 \times 10^{-6}$ $m^2$), and *k* is the dielectric constant, 3.9 for $SiO_2$ and $k_0 = 8.854 \times 10^{-12}$ $Fm^{-1}$ for free space.[27] The obtained dielectric constant, 179, is much larger than that for the as-deposited film, approximately 43 (thickness: 206.0 nm by ellipsometry), possibly because the as-deposited film is not of pure STO but composed of complex compounds, and it was an amorphous film.

However, the C−V plot also shows a large flat-band voltage shift of about −2.0 V (corresponding to approximately 0.1 $MVcm^{-1}$) along the voltage axis between the accumulation state and the inversion region, which is unacceptable for MOS applications. The flat-band voltage shift is sensitive to annealing conditions either in an oxygen atmosphere or a hydrogen environment.[28] The voltage shift in this case indicates the presence of positive charges in the oxide−semiconductor interface with a high surface state density of at least $6.7 \times 10^{12}$ states·$cm^{-2}$.[27] The source of such fixed charge is thought to originate from the detailed bonding of the atoms associated with the dielectric near the dielectric/semiconductor interface. The origin of this shift is considered to be associated with oxygen vacancies, which are positively charged. It is reported (ref 1a and references therein) that the existence of excess Sr at a condition of Sr/Ti > 1 and excess Ti at Sr/Ti < 1 induces the oxygen vacancy with two compensation electrons ($V^{\cdot}_{\cdot O}$) from the viewpoint of defect chemistry, expressed by the Kröger−Vink notation:

$$SrO = V''''_{Ti} + Sr^{\times}_{Sr} + O^{\times}_{O} + 2V^{\cdot\cdot}_{O} \quad (Sr/Ti > 1)$$

$$TiO_2 = V''_{Sr} + Ti^{\times}_{Ti} + 2O^{\times}_{O} + V^{\cdot\cdot}_{O} \quad (Sr/Ti < 1)$$

For our as-deposited films (AHFT/SN was 1/1), the XPS result of Sr/Ti was 1.0/1.07 for a measured sample,

(25) Jolivet, J−P.; Henry, M.; Livage, J. *Metal Oxide Chemistry and Synthesis*; John Wiley & Sons: New York, 1994.
(26) Niesen, T. P.; Bill, J.; Aldinger, F. *Chem. Mater.* **2001**, *13*, 1552.
(27) (a) Grove, A. S. *Physics and Technology of Semiconductor Devices*; John Wiley & Sons: New York, 1967. (b) Sze, S. M. *Physics of Semiconductor Devices*; John Wiley & Sons: New York, 1969.
(28) Guha, S.; Cartier, E.; Gribelyuk, M. A.; Bojarczuk, N. A.; Copel, M. C. *Appl. Phys. Lett.* **2000**, *77*, 2710.

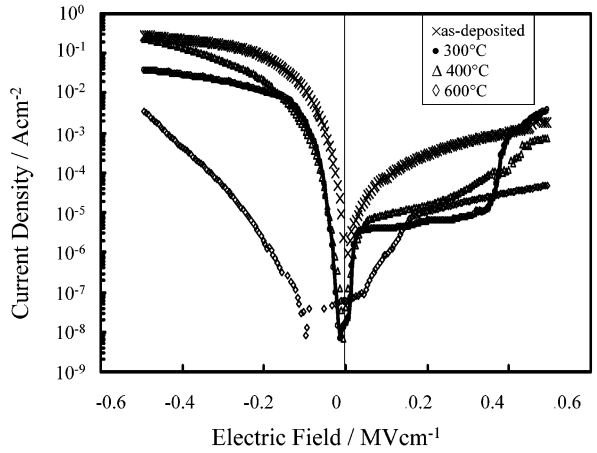


**Figure 11.** I−V characteristics of MOS devices with the as-deposited STO precursor solid thin film and those annealed as gate films.

showing that the film is nonstoichiometric at least in the measured surface layer of the film according to XPS analysis limit in depth (< 2 nm). The defect reactions mentioned above may bring about oxygen vacancies, which might act as electron donors and cause poor electrical properties.

Figure 11 shows the I−V characteristic of the as-deposited film and those after annealing at different temperatures for 2 h in air. All the curves of Figure 10 demonstrate asymmetric nonlinear resistance consistent with the rectification effect of a MOS structure. The current density increased quickly with increasing bias voltage when the device was in the ON state. However, no obvious increase can be observed in the OFF state. Because p-type silicon was used as the substrate, higher leakage current was obtained at the negative bias voltage when the depletion layer generated at the Si surface contacted the oxide layer. The leakage current decreased with increasing annealing temperature. The corresponding value of leakage current at 1.0 V (corresponding to 49 $kVcm^{-2}$) for the film annealed at 600 °C was reduced by 2 orders of magnitude as compared with that of the as-deposited film. This result suggests that insulating properties can be significantly improved by high-temperature annealing. It is also evident that the leakage current is closely related to the annealing process, especially to the crystallization of STO film. Comparing the AFM images of an as-deposited film with those of an annealed one shows that crystallization at 600 °C resulted in grain growth and densification, leading to the reduction of grain-boundary leakage current. The resistivity and leakage current density at 1.0 V (corresponding to 49 $kVcm^{-1}$) of the MOS device evaluated by using a crystalline film as a gate oxide layer are $4.11 \times 10^{11}$ Ωcm and $1.19 \times 10^{-7}$ $Acm^{-2}$, respectively. At −1.0 V (at $V_{bias} = V_{FB} + 1$ V), the leakage current was as low as $3.21 \times 10^{-8}$ $Acm^{-2}$. However, the resistivity is still low compared to a typical gate dielectric (>$10^{13}$ Ωcm), and the leakage current must be further suppressed to below $10^{-8}$ $Acm^{-2}$. The poor qualities of our films are possibly due to their nonstoichiometric composition, giving rise to high densities of electron donors which would lead to low resistivity and high leakage current.

We mainly investigated how various characteristics of STO films and MOS structure were affected by annealing temperature, which are important for application of our films to conventional MMIC or MOSFET processes. It was concluded that crystallization had great effects on the reduction of leakage current and the increase in dielectric constant, whereas the annealing conditions still need to be optimized. These foundations also suggest it is necessary to carefully control the molar ratio of Sr/Ti in the STO film during the film deposition in order to achieve high dielectric performance by the LPD method. Doping the film with acceptor elements may be another way to compensate the oxygen vacancies and improve the dielectric properties. Approaches to the control of surface charge instability have been reported through modification of the oxide film by lightly doping STO with acceptor elements, such as Fe, Al, Mn, and Cr.[29] Acceptors of low concentration in Ti sites electrically compensate for donor species such as oxygen vacancies observed in undoped STO films, greatly reducing the leakage current by both increasing the Schottky barrier height at the substrate−oxide interface and expanding the depletion layer width. However, donor-type substitution, either La for Sr sites or Nb for Ti sites, increases the concentration of residual conduction electrons, leading to a significant increase in leakage current. Postannealing the as-deposited film under an oxygen atmosphere may have an effect similar to that of the addition of dopants because oxygen vacancies would become filled with oxygen ions. Further studies are being made to improve the dielectric properties based on these ideas. Once the leakage current falls within acceptable limits, the STO deposited by a combination of the LPD method with the SAM technique will become a promising candidate for dielectric thin film materials.

## 4. Conclusions

A novel method, using a simple apparatus and easily achieved conditions, has been developed for the preparation of STO micropatterns and thin films through a one-step process at ambient temperature by combining the LPD method with the SAM technique. The films were selectively deposited in the silanol regions of HFDTS-SAMs. The as-deposited film was amorphous, containing fluorine as a main impurity. After annealing at 500 °C for 2 h in air, the as-deposited film was crystallized into $SrTiO_3$ and the fluorine was eliminated. Film morphology was characterized by both SEM and AFM, and an Ostwald ripening growth mode was suggested. MOS (metal-oxide-semiconductor) devices were prepared using an as-deposited film or a crystallized film as a gate oxide, respectively. The dielectric constant of $SrTiO_3$ thin films, leakage current, and impedance properties of the MOS device were evaluated. This research indicates that STO films prepared by a combination of LPD and SAM techniques are promising for microelectronics applications.

CM020358P

(29) (a) Kim, S.; Park, C. *Appl. Phys. Lett.* **1999**, *75*, 2554. (b) Copel, M.; Baniecki, J. D.; Duncombe, P. R.; Kotecki, D.; Laibowitz, R.; Neumayer, D. A.; Shaw, T. M. *Appl. Phys. Lett.* **1997**, *73*, 1832.